Materials Science in Semiconductor Processing 41 (2016) 390–397

Contents lists available at ScienceDirect

Materials Science in Semiconductor Processing

journal homepage: www.elsevier.com/locate/mssp

Effect of deposition temperature on polymorphous silicon thin films by PECVD: Role of hydrogen

L. Hamui [a,e], B.M. Monroy [a], K.H. Kim [b,c], A. López-Suárez [d], J. Santoyo-Salazar [e], M. López-López [e], P. Roca i Cabarrocas [b], G. Santana [a,*]

[a] Instituto de Investigaciones en Materiales, Universidad Nacional Autónoma de México, A.P. 70-360, Coyoacán, C.P. 04510 México, D.F., México
[b] Laboratoire de Physique des Interfaces et des Couches Minces, CNRS, Ecole Polytechnique, 91128 Palaiseau, France
[c] Korea Institute of Energy Research-KIER-UNIST Advanced Center for Energy, Ulsan, South Korea
[d] Instituto de Física, Universidad Nacional Autónoma de México, A.P. 20-364, Coyoacán, C.P. 04510 México, D.F., México
[e] Departamento de Física, Centro de Investigación y de Estudios Avanzados, A.P. 14-740, Gustavo A. Madero, México, D.F., México

ARTICLE INFO

Article history:
Received 27 August 2015
Received in revised form
3 October 2015
Accepted 3 October 2015

Keywords:
Polymorphous silicon
Hydrogen bonding
Exodiffusion
AFM
Optical properties

ABSTRACT

Pm-Si:H which has improved optical and transport properties as well as stability compared to hydrogenated amorphous silicon is studied. In order to understand the effect of the growth temperature on pm-Si:H films, hydrogen bonding and stability were analyzed in this work. Samples grown at different temperatures were compared and a change on the films morphology and structure was observed. HRTEM images evidence nanocrystals with approximate size of 9 nm. A growth surface reorganization was observed at an almost constant deposition rate. Increasing the deposition temperature leads to a more ordered, compact and smooth structure of the pm-Si:H films. Hydrogen interaction with the growing surface is related to the deposition temperature, changing the growth of the amorphous matrix due to hydrogen surface diffusion into lower energy and more stable positions. The total hydrogen in the film is reduced as temperature increases and hydrogen becomes more tightly bonded, which changes in a non monotonous way how the nanocrystals are incorporated and their environment. The optoelectronic properties of the films are directly related to the incorporation of hydrogen and whether it is weakly or tightly bonded. A diminution of the optical gap of the pm-Si:H films in the range from 1.71 to 1.65 eV was observed with the increase of the deposition temperature in the range from 175 to 275 °C.

1. Introduction

In recent years hydrogenated amorphous silicon (a-Si:H) has been the base material for the manufacturing of large area electronic devices such as TFT's (thin film transistors), which are the basis for expanding flat panel industries. This is a consequence of the combination of low material consumption, large area deposition and low temperature process which results in low production costs. Various techniques have been used to optimize plasma enhanced processes to manufacture hydrogenated amorphous silicon PIN devices, thus obtaining conversion efficiencies of up to 10.1% [1] for single junction solar cells, but theoretically efficiencies as high as 19% can be achieved [2]. In spite of this, hydrogenated amorphous silicon has a light-induced degradation effect referred to as the Staebler–Wronski Effect (SWE) [3]. The SWE is understood as the light-induced creation of metastable defect states (associated with the rupture of Si–Si weak bonds), which then act as recombination centers, greatly reducing the efficiency during device operation [4,5]. To address this problem, several solar cell structures with double and triple junction have been investigated allowing to reach 16.3% initial [6] and 13.5% [7] stabilized efficiencies. These efforts increase the conversion efficiency but the device degradation remains a limiting factor. Hydrogenated polymorphous silicon (pm-Si:H), which consists of nanocrystals embedded in an amorphous matrix, shows greater stability under illumination, better electronic properties and lower defect density than a-Si:H [8,9] and thus is an attractive material for solar cells applications [4,8,10].

In pm-Si:H the optical properties are similar to those of hydrogenated amorphous silicon and the transport properties are improved, in particular hole mobility and stability [11,9], due to the medium range order in the material caused by the inclusion of nanocrystals and their effect on the surrounding environment [12]. The structural disorder of the amorphous matrix is significantly reduced by the presence of silicon nanocrystals and how they are

* Corresponding author.
E-mail address: gsantana@iim.unam.mx (G. Santana).

http://dx.doi.org/10.1016/j.mssp.2015.10.005
1369-8001/

immersed in the film [10,13] improving transport properties. Since the size and density of the nanocrystals embedded in the amorphous matrix can be controlled, it is possible to obtain changes on the optoelectronic properties of these materials [13]. However, the hydrogen bonding configuration can be more complex since hydrogen can be found in the amorphous matrix and in the nanocrystalline/amorphous interface [14].

Due to the important role of hydrogen in these materials [15,16], hydrogen bonding and stability should be analyzed, and knowledge about hydrogen bonding environment and configuration within the film structure is relevant. A detailed study of this aspect is important in terms of the stability of pm-Si:H thin films in solar cells. In this paper, the influence of the growth temperature on the hydrogen bonding of pm-Si:H thin films deposited at high rate (5.2–6.3 Å/s) is studied by means of exodiffusion experiments, atomic force microscopy (AFM), spectroscopic ellipsometry (SE), elastic recoil detection analysis (ERDA) complemented with Rutherford Backscattering Spectrometry (RBS) and Fourier transform infrared spectroscopy (FTIR). The morphological and optoelectronic properties of the films are also discussed in terms of their relationship with the growth temperature.

2. Materials and methods

Pm-Si:H thin films were deposited on corning glass #7059 substrates using the plasma enhanced chemical vapor deposition technique (PECVD) in the ARCAM system [17]. The deposition was done with a chamber pressure of 3.3 Torr and a RF power of 30 W, leading to relatively high deposition rate (5.2–6.3 Å/s) as shown in Table 1. Hydrogen (H_2) and silane (SiH_4) were used as precursor gases with mass flow rates of 200 and 40 sccm, respectively. Pm-Si:H films deposited at various substrate temperatures (175, 210, 240 and 275 °C) have been studied. Atomic force microscopy measurements were conducted using a Jeol JSPM-4210. Samples were measured using the intermittent contact mode on a 1 squared micrometer surface for the roughness analysis. SE measurements were conducted using a HORIBA Jobin–Yvon UVISEL in order to determine the films thickness, surface roughness and optical properties such as the absorption coefficient (α) and the optical gap (E_g).

The real (ε_1) and imaginary (ε_2) parts of the pseudo-dielectric function can be derived by using the Kramers–Kroning relations as described elsewere [18]. The dielectric function conversion to the refractive index (n) and extinction coefficient (k) are as follows:

$$n = \sqrt{\frac{[\varepsilon_1 + \sqrt{(\varepsilon_1^2 + \varepsilon_2^2)}]}{2}} \tag{1}$$

$$k = \sqrt{\frac{[-\varepsilon_1 + \sqrt{(\varepsilon_1^2 + \varepsilon_2^2)}]}{2}} \tag{2}$$

Table 1
Effect of substrate temperature on the deposition rate, crystalline fraction, structure factor and nanocrystals surface passivation.

Sample	Temperature (°C)	Depo. rate (Å/s)	Crystalline fraction (Xc) (%)	Structure factor (%)	Nanocrystals surface passivation index (%)
1007084	175	6	12.80	41.50	31.10
1007073	210	6.3	11.40	33.00	32.30
1007087	240	5.2	11.50	27.60	18.10
1007089	275	6.1	14.00	8.80	26.60

where

$$\varepsilon_1 = n^2 - k^2 \tag{3}$$

$$\varepsilon_2 = 2nk \tag{4}$$

The Forouhi–Bloomer dispersion equations relates the refractive index and extinction coefficient to the real and imaginary part of the pseudo-dielectric function for an amorphous material as a function of energy as follows [19]:

$$k(E) = \frac{A(E - E_g)^2}{E^2 - BE + C} \tag{5}$$

$$n(E) = n(\infty) + \frac{\left\{\frac{A[\frac{-B^2}{2} + E_gB - E_g^2 + C]}{\frac{1}{2}\sqrt{(4C + B^2)}}\right\}E + \left\{\frac{A[\frac{B}{2}(E_g^2 + C) - 2E_gC]}{\frac{1}{2}\sqrt{(4C + B^2)}}\right\}}{E^2 - BE + C} \tag{6}$$

where A, B, C, and E_g are material parameters for model adjustment.

Moreover, the absorption coefficient can be described by the following equation:

$$\alpha = \frac{4\pi k}{\lambda} \tag{7}$$

A Tauc–Lorentz model was selected in order to obtain the optical and morphological model parameters of the films. This model is a result of the equation of the Tauc joint density of states multiplying the equation of the Lorentz oscillator (for a single oscillator) which gives the following equation for the imaginay part of the dielectric function (ε_{2TL}):

$$\varepsilon_{2TL}(E) = \begin{cases} \frac{A \cdot E_0 \cdot C \cdot (E - E_g)^2}{E((E^2 - E_g)^2 + C^2 \cdot E^2)} & E > E_g \\ 0 & E < E_g \end{cases} \tag{8}$$

where E_0 is the peak transition energy, E_g is the gap energy, C the broadening parameter and A the height of the imaginary part of the dielectric function. The Tauc–Lorentz model parameters C and A are related to the film disorder and to the film compactness, respectively [20]. A 3 layer stack model was selected in order to describe the film which consist of a surface layer composed of voids and material, a second layer that represents the pm-Si:H film and a third layer which is the substrate. The voids fraction was calculated from the optical model fitting the surface layer. Raman spectroscopy was used to investigate the nanostructure of the films via a Jobin Yvon T6400 micro-Raman spectrometer equipped with a He–Ne laser (632.8 nm) excitation. A low incident power (2 mW) was selected in order to avoid any beam-induced structural changes during measurements. The crystalline fraction was obtained from the analysis of different phonon modes between 400 and 550 cm^{-1}. Raman spectra were decomposed into three bands related to the amorphous phase (480 cm^{-1}), an intermediate phase (500–517 cm^{-1}) related to small size nanocrystals and grain boundaries, and a crystalline phase (520 cm^{-1}) [10,21,22]. High resolution transmission electron microscopy (HRTEM) measurements were conducted at CINVESTAV-IPN. Each thin film sample was prepared in a carbon–copper lacey grid, 400 mesh for HRTEM characterization. First, the film was removed from the substrate by scraping. Then the film was supported over the grid surface. Bright field images were obtained from the films in a transmission electron microscope JEOL-JEM 2010 at 200 kV and 105 μA. The amorphous and crystalline contributions in the films were analyzed by selected area electron diffraction (SAED) at

camera length of 20 cm.

Exodiffusion experiments were performed in a vacuum chamber with a controlled heating system which increases the temperature by 10 °C/min, and the effusing hydrogen was detected with a mass spectrometer. Hydrogen pressure was normalized to the film volume to compare between the films. A decomposition into 4 Gaussian peaks was done in order to determine the hydrogen environment in pm-Si:H. Weakly bonded hydrogen corresponding to the pm-Si:H network and the surface of silicon nanocrystals effuses from the peaks around 350 and 410 °C, respectively. The large band around 500 °C can be related to tightly bonded hydrogen within the amorphous network, while the band at 572 °C corresponds to hydrogen evolving from the nanocrystals surface [23]. The hydrogen content of the films was measured by ERDA. During the ERDA analysis, the samples were irradiated with a collimated 3 MeV α-particle of 1.5 mm diameter, using the Instituto de Física, UNAM 3 MV 9SDH-2 Pelletron accelerator. The surface of the sample was placed at an angle of 15° with respect to the incoming beam. A surface barrier detector, used to detect the hydrogen recoils, was placed at an angle of 30° with respect to the beam direction. A 12 μm thick Mylar ($C_{10}H_8O_4$) foil was used in front of the detector to stop elastically scattered ions heavier than recoiled hydrogen. Simultaneously, Rutherford backscattering spectroscopy (RBS) measurements were carried out in order to quantify the integrated charge deposited on the sample during the ERDA measurements. The energy of the backscattered particles was recorded with a silicon surface barrier detector positioned at a scattering angle of 167°, using the same particle accelerator as for the ERDA experiment. The simulation and analysis of both RBS and ERDA spectra were done using the SIMNRA code [24]. To simulate the ERDA spectra the profile of atomic concentrations corresponding to the sample composition, measured by RBS, was taken into account. The hydrogen concentration was obtained from the sum of hydrogen surface concentrations (atoms/cm^2) detected by ERDA. The integration of surface concentrations in depth, over the whole film thickness, results in the total atomic hydrogen concentration (atoms/cm^3). Fourier transform infrared measurements were conducted in the attenuated total reflectance (ATR) configuration in a Nicolet 510 spectrometer. To study the hydrogen incorporation in the films the Si–H stretching band between 1900 and 2200 cm^{-1} was selected and decomposed into three peaks. The peaks around 1990 and 2090 cm^{-1} correspond to the monohydride (Si–H) and polyhydride bonding (Si–H_n) configurations, respectively. The latter peak could be associated to clustered hydrogen passivating the walls of nanovoids while the band around 2030 cm^{-1} is related to hydrogen passivating the surface of the silicon nanocrystals [8,14]. Then, the structure factor, which is the ratio of the 2090 cm^{-1} band to the total stretching band [8,25], and the nanocrystals surface passivation index, which is ratio of the 2030 cm^{-1} band to the total stretching band were obtained for further analysis. The structure factor is related to the amount of disorder in amorphous network while the 2030 cm^{-1} ratio is related to the presence of nanocrystals in pm-Si:H films.

3. Results

Table 1 shows the deposition rate, crystalline fraction and structure factor as functions of the deposition temperature. The deposition rate is around 6 Å/s, except for the sample grown at 240 °C. From the decomposition of the Raman spectra the crystalline fraction (Xc) was obtained as a function of the deposition temperature. The Xc varied in the range of 11–14% for the studied films, not showing any trend. The structure factor was obtained from the FTIR hydrogen vibration modes which give us additional information about the hydrogen bonding configuration in the films.

Table 2
Spectroscopic ellipsometry results as a function of the substrate temperature.

Temperature (°C)	Film thickness (nm)	Surface roughness (nm)	Voids fraction in the surface roughness (%)	E_g (eV)	A	C
175	174.18	6.24	28.71	1.71	213.92	1.89
210	182.82	6.31	26.13	1.71	224.82	1.90
240	148.67	6.37	21.18	1.68	222.17	1.91
275	175.71	6.88	19.68	1.65	215.87	1.88

The structure factor decreases from 41.5% to 8.8% with the deposition temperature as shown in Table 1. The nanocrystals surface passivation index is observed to increase with temperature however it shows a steep decrease for the sample deposited with 240 °C from 32.3% (210 °C) to 18.1% (240 °C). Table 2 shows the optical and morphological model parameters obtained by SE as a function of the deposition temperature using a Tauc–Lorentz model for the films. As the deposition temperature increases the void fraction in the surface roughness decreases. While its thickness shows a very small but increasing variation with the temperature. The optical gap decreases from 1.71 to 1.65 eV with increasing deposition temperature. The Tauc–Lorentz disorder parameter C is found to be very similar for all the samples. The film compactness parameter A shows an initial increase with temperature indicating a higher density, but it decreases for temperatures above 210 °C. In order to study the surface morphology of the films more precisely, AFM measurements were performed and the average height of the surface roughness of the samples was analyzed as shown in Fig. 1. The AFM images show that as the deposition temperature is increased the surface morphology becomes smoother with smaller surface roughness. In addition, as we set the deposition temperature to higher values, the average height of the surface roughness decreases from 14 nm to 4 nm.

The Raman spectra was decomposed into several peaks associated to the phonon modes of the pm-Si:H as shown in Fig. 2 for the 175 °C sample. HRTEM measurements show the evidence of silicon nanocrystals in the amorphous matrix as shown on Fig. 3a for the sample deposited at 175 °C where the crystalline and amorphous phases are observed. Fig. 3b shows the crystalline planes of the nanocrystals that have an approximate size of 9 nm. Also, in Fig. 3c the diffraction patterns of the HRTEM image is shown, where it is possible to appreciate mainly an amorphous material with a small order. Fig. 4 shows a plot of hydrogen pressure that effused from the films as a function of the annealing temperature for all the samples. Firstly, it is possible to appreciate that changing the deposition temperature produces an evident variation in the quantity of hydrogen that is effusing from the films which, as expected, is reduced with increasing deposition temperature. Second, for the samples deposited at the lowest substrate temperatures a shoulder around 350 °C is observed. The intensity of the exodiffusion spectra decreases along with a reduction of the shoulder around 350 °C with increasing deposition temperature. Also, in Fig. 4a decomposition of one exodiffusion spectra into 4 Gaussian peaks (350, 410, 500 and 570 °C) is shown [14,23,26]. This was done to analyze the environment where hydrogen comes from, and also to distinguish between hydrogen effusing from tight and weak bonds. The first two peaks of the decomposition are associated to weakly bonded hydrogen in the amorphous matrix and on the nanocrystals surface (350, 410 °C), respectively, while the following two peaks are related to tightly bonded hydrogen that evolves from the amorphous matrix and from the nanocrystals surface (500, 570 °C), respectively [23,27].

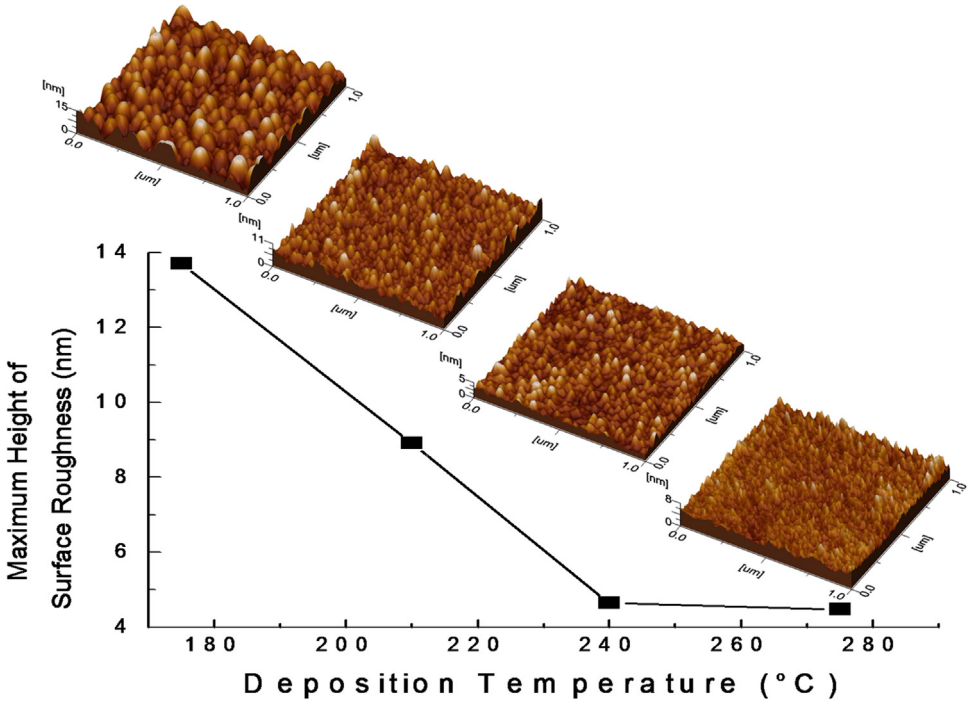

Fig. 1. Surface roughness as a function of substrate temperature with AFM morphology insets for every sample.

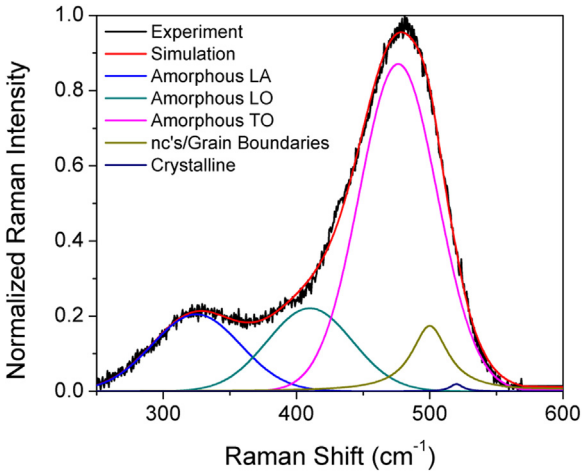

Fig. 2. Representative Raman spectra and its decomposition for the pm-Si:H film grown at 175 °C.

The total amount of effusing hydrogen is shown in Fig. 5a as a function of the deposition temperature. A decreasing trend of the hydrogen effusing from the films is shown. The weakly and tightly bonded hydrogen percentage plot is shown (Fig. 5b) in order to determine the bonding environment of the hydrogen that is effusing from the films. This percentage was obtained dividing independently the amount of weakly and tightly bonded hydrogen by the total amount of hydrogen effusing from the films. A slight decrease in the tightly bonded hydrogen from 60% to 55% is observed followed by an increasing trend up to 70%, and all of this is opposite to the weakly bonded hydrogen behavior.

The spectra of the Si–H stretching band between 1900 and 2200 cm^{-1} for each deposition temperature and also a decomposition of the band is shown in Fig. 6. One can see that the stretching band intensity is reduced with deposition temperature to very low values for the films grown at 240 and 275 °C. As the deposition temperature is increased the band around 2090 cm^{-1} is significantly decreased.

Fig. 7 shows the percentage of weakly and tightly bonded hydrogen on the surface of nanocrystals obtained from exodiffusion spectra as a function of the deposition temperature. This fraction is obtained from the ratio of the respective Gaussian peaks (410 °C and 570 °C) to the total spectra. Weakly bonded hydrogen increases with temperature up to 35% and for temperatures above 240 °C it decreases again to 32%, while tightly bonded hydrogen first increases from 2% to 3.5% and then, at higher temperatures it decreases linearly down to almost 2.2% for the 275 °C sample. Fig. 8 shows the hydrogen depth profile obtained by ERDA for the sample deposited with the lowest temperature (175 °C). Simulation of the spectra was performed with the SIMNRA program using both ERDA and RBS measurements. The simulation results for all the samples show that the hydrogen concentration is reduced in depth as observed in Fig. 8. It can be observed that the hydrogen concentration varies from 0.38 to 0.015 with depth with an important diminution ~130 nm. A table showing the hydrogen density as a function of the deposition temperature was added as an inset in Fig. 8. It is observed that all the samples have a hydrogen concentration of approximately 2×10^{22} atoms/cm^3 which agree with the reported concentrations in hydrogenated amorphous silicon [28,29].

To study the film optical properties, the refractive index (n) and the extinction coefficient (k) spectra are shown in Fig. 9 deduced from the ellipsometry model described above. It is worth to notice that the curves of n and k show an increase with temperature and it is more pronounced for the n spectra. There is a gap between the first temperature and the next three for the refractive index.

4. Discussion

First we have to notice that the change in the deposition temperature is accompanied by a drastic change in the surface morphology of the film during deposition as observed in Fig. 1. Larger cluster grain sizes and heights are favored with low deposition temperatures and the opposite is observed at higher deposition temperatures. The surface becomes smoother with

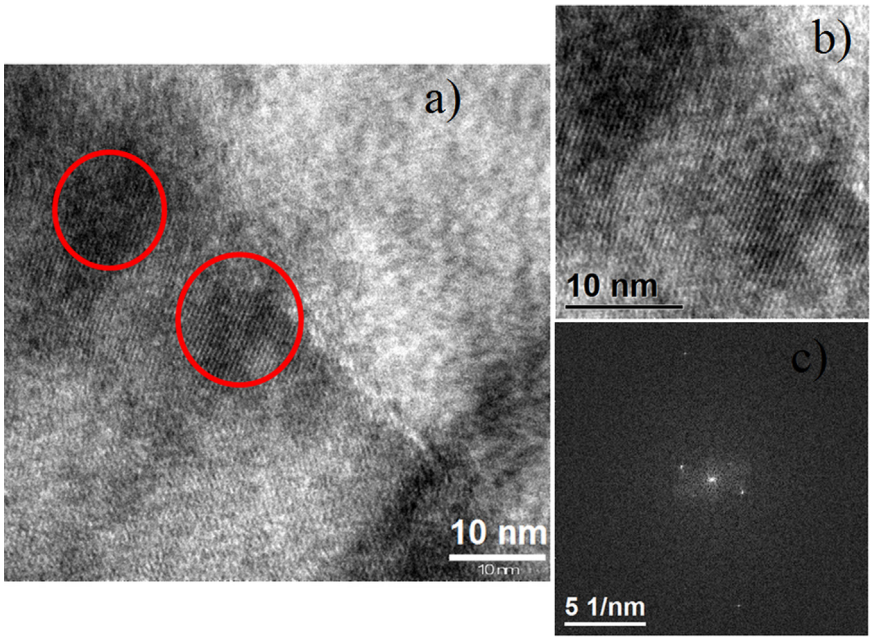

Fig. 3. a) HRTEM image from pm-Si:H film for the deposition temperature of 175 °C where the crystalline and amorphous phases are observed. b) Magnification of the crystalline phase and also c) the diffraction pattern of the HRTEM image.

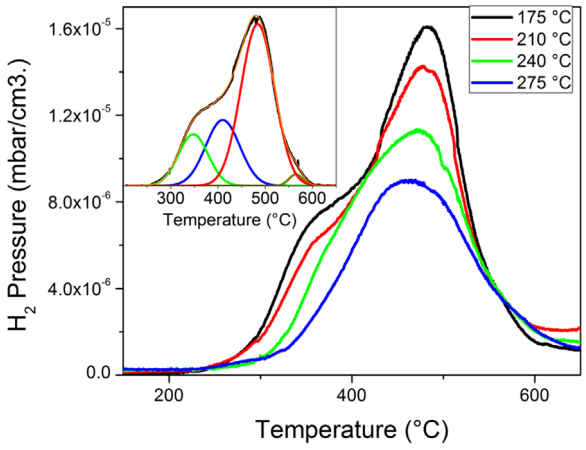

Fig. 4. Exodiffusion spectra measured for samples deposited with different substrate temperatures. The inset shows a decomposition of the spectrum for the film grown with 175 °C.

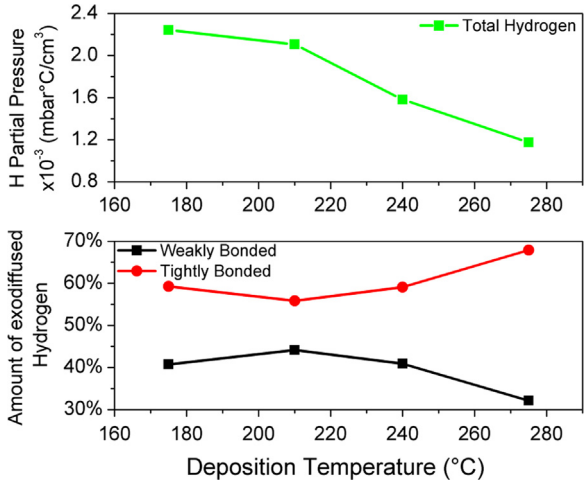

Fig. 5. a) Total exodiffused hydrogen and b) amount of exodiffused hydrogen from tightly (500, 570 °C) and weakly (350, 410 °C) bonded positions as a function of deposition temperature.

smaller grain sizes. The average height of the surface roughness decreases, but the average surface roughness determination by SE (Table 2) stays between 6 and 7 nm. The film growth changes because at lower deposition temperatures a columnar growth is favored [30] while at higher deposition temperatures it tends to a more homogeneous deposition (Fig. 1). These changes as a function of temperature could be explained in terms of the different radical surface mobility during growth. At these deposition temperatures the surface diffusion is a thermally activated process between two adsorption sites separated by a large energy barrier close to the binding energy. Atomic hydrogen has a determining role in the creation of nucleation sites. If hydrogen atoms do not have the necessary energy to overcome the barrier, two scenarios may be present. In the first one, hydrogen could be bonded in the first adsorption site passivating the surface or, in the second one, hydrogen is not bonded in this position and a desorption process takes place. The additional thermal energy present at higher deposition temperatures contributes to the atoms movement over the growth surface, favoring displacements of radicals into minimal energy positions homogeneously distributed on the surface [31–33]. Thus a less stressed environment is expected and a better arrangement of the silicon atoms in the growing film is obtained. As a consequence, hydrogen is preferentially incorporated as tightly bonded Si–H for higher temperatures (Fig. 5b) and the amorphous matrix presents less hydrogen voids (Table 2) and defects. On the other hand, the structure factor (Table 1), which is commonly associated to the amount of disorder in a-Si:H films [25], decreases with increasing deposition temperature.

It has been discussed in previous works that the silicon nanocrystals are formed in the plasma and incorporate to the growing surface [34–37]. Since nanocrystals are formed within the plasma, their nucleation and growth are determined by the plasma chemistry. When they escape the plasma region they are deposited on the growing film surface [8,10,34–36].Thus, their average size is expected to be independent of the substrate temperature [13]. However, the substrate temperature modifies the arrangement,

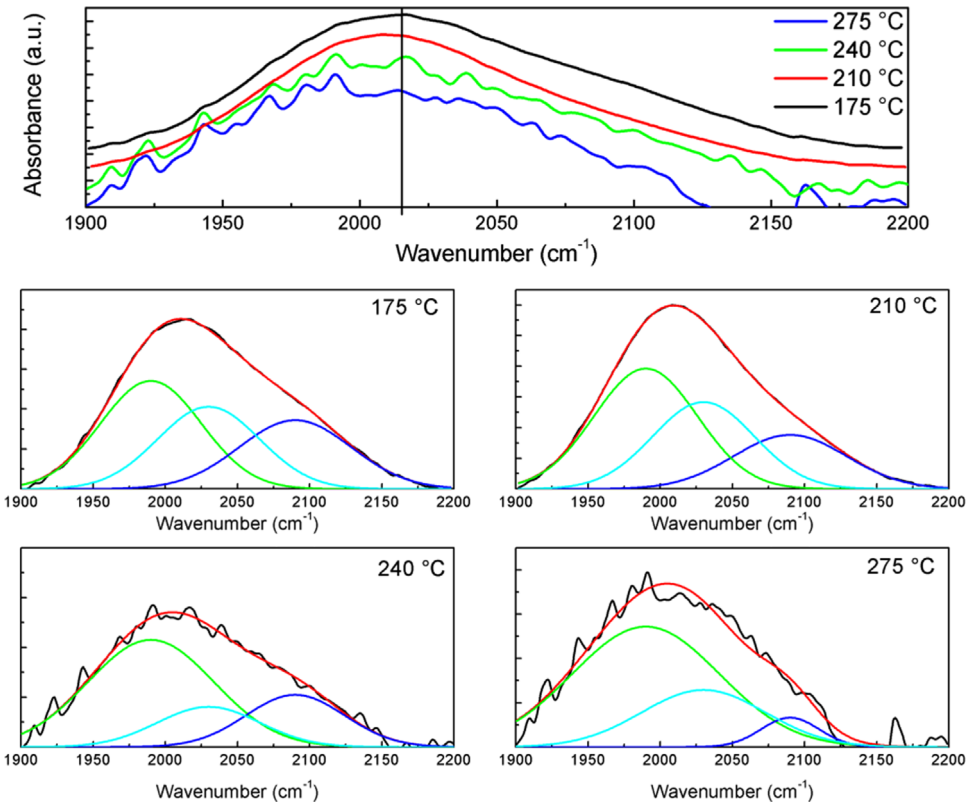

Fig. 6. Absorbance FTIR spectra corresponding to the Si–H stretching band for the different deposition temperatures showing a shift to lower wavelengths and their decomposition.

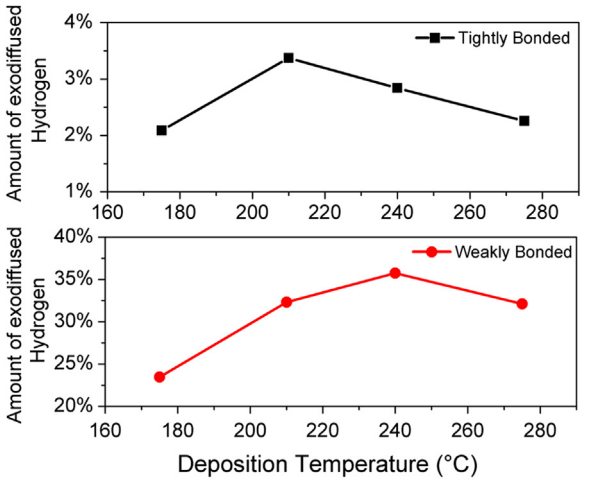

Fig. 7. Amount of tightly and weakly bonded hydrogen exodiffused from nanocrystals surface as a function of the deposition temperature.

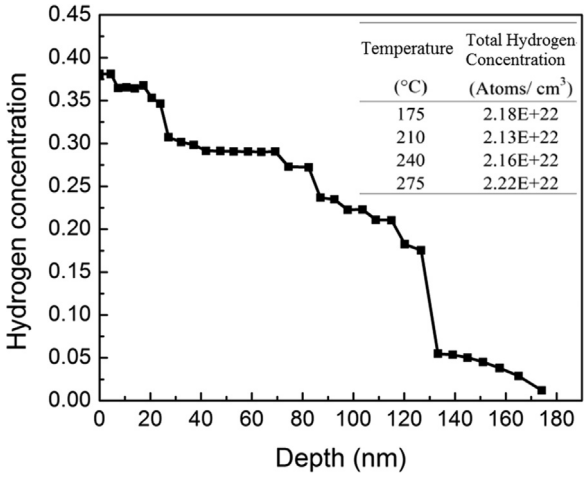

Fig. 8. ERDA hydrogen concentration depth profile for the sample grown at 175 °C and total hydrogen concentration as a function of the substrate temperature.

morphology, stress and passivation of the amorphous matrix and, therefore, how the nanocrystals are surrounded or the environment in which they are located. We assume that the increase in the deposition temperature affects mainly the growth of the amorphous matrix and the way it surrounds the nanocrystals, since the plasma conditions are constant for this set of samples.

Exodiffusion experiments show an evident variation in the quantity of hydrogen that is effusing from the films. For the samples deposited at the lowest substrate temperatures a shoulder around 350 °C is observed related to the structure factor (Table 1) which decreases with temperature. The amount and type of bonded hydrogen in the pm-Si:H films affects the surface roughness and compactness of the films. A displacement of the exodiffusion peak toward higher annealing temperatures indicates that the energy is minimized in order to obtain tighter bonding, avoiding hydrogen effusion (Fig. 4) that could cause film degradation by the SWE.

Several models have been previously proposed to explain the pm-Si:H growth [12,25,26] but we focus on the surface diffusion model. In the surface diffusion model, high H flux impinging on the surface enhances the mobility of the deposited precursors [39]. In this case, the low temperature shoulder around 350 °C is attributed to both the rupture of Si–H groups located on the surfaces of internal voids and the simultaneous formation of H_2 molecules that evolve from an interconnected void network [27] in the amorphous matrix. Another possibility is that hydrogen trapped as

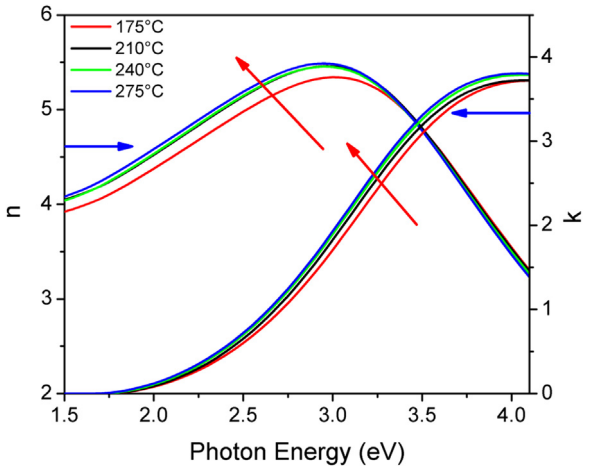

Fig. 9. Variation with temperature of the refractive index and extinction coefficient after modeling of SE spectra.

H_2 molecules diffuses from connected microvoids to the surface as the annealing temperature increases. This explanation is consistent with the morphology observed by AFM, FTIR and spectroscopic ellipsometry. Films deposited at low temperatures show a columnar-type growth of clusters and not a homogeneous and dense structure, which would favor this kind of effusion.

Of special interest is the FTIR band around 2030 cm^{-1}, which has been previously shown to be a signature of pm-Si:H films and indicative of the existence of silicon nanocrystals in an amorphous matrix [8]. This band is related to hydrogen bonds passivating the surface of small crystals produced in the gas phase and incorporated into the silicon matrix. It is observed that the percentage of this peak with respect to the total stretching band stays between 18% and 32% (Table 1). However, the 240 °C sample shows an important decrease which indicates that the nanocrystals surface passivation changes due to the effect of the substrate temperature. Weak bonds on the nanocrystals surface break and then diffuse to the amorphous silicon matrix or are desorbed during growth. This hydrogen passivates the dangling bonds within the film and the adsorption sites in the growing surface. This limits the adsorption process of silicon radicals compromising the film growth and explaining the reduction of the film thickness for this temperature. The weakly bonded hydrogen diffuses or even effuses and the remaining hydrogen within the film turns out to be more stable for this temperature.

We propose that the breaking of the nanocrystals hydrogen passivation bonds causes the surface silicon atoms to bond with the silicon atoms in the amorphous matrix, indicating a different incorporation of the nanocrystals in the film and resulting in a more ordered structure at medium range. Previous works have related the weakly bonded hydrogen at the surface of nanocrystals with clustered Si–H bonds or $(Si–H_2)_n$ chains at grain boundaries [38,40]. One of the probable solid state reactions that could explain this kind of hydrogen effusion is [38]:

$$Si - H\,H - Si \longleftrightarrow Si - Si + 2H\,(\text{mobile}) \quad (10)$$

In other words, nearby Si–H bonds at the surface of silicon nanocrystals would enhance surface reorganization and hydrogen effusion even at low annealing temperatures. Also, a higher amount of clustered Si–H bonds is expected to occur in films with connected microvoids or columnar growth. Therefore, this interpretation is consistent with our AFM, FTIR and SE results for films deposited at low temperatures. On the other hand, when the film microstructure becomes compact as the ones obtained for the films deposited above 200 °C (Table 2), hydrogen apparently remains more weakly bonded in the surface of the nanocrystals (Fig. 7).

Table 2 shows a decrease on the optical gap values from 1.71 to 1.65 eV in agreement with previous works [41]. This variation in the optical band gap is mainly determined by the hydrogen content and its bonding environment in the film. Having in mind the application of this material in solar cell devices, the absorption coefficient was obtained and a slight red shift was observed with the deposition temperature. However, the obtained curves show that all the analyzed films are in a range close to the amorphous silicon reference materials. A less dense structure could lead to a material with lesser effective absorption coefficient. In our case, the density of the film increases with temperature explaining the slight changes in the absorption coefficient, which confirms that the film's deposition temperature plays an important role on the optical properties. It was demonstrated that for a-Si:H the optical bandgap and the refractive index at long wavelenghts are sensitive to the hydrogen concentration [42] due to the bond polarizabilities [43] and hydrogen binding resulting from deposition [44]. The refractive index is also sensitive to the microstructure and structural defects of the material [42]. The gap between the first temperature and the next three observed in Fig. 9 is correlated to a diminution of micro-voids in the amorphous network. A higher value of the structure factor, observed at lower temperatures, indicates a larger amount of $Si–H_2$ which corresponds to an open material structure and therefore a lower refractive index.

5. Conclusions

Increasing the deposition temperature leads to a more ordered, compact and less voided structure in the pm-Si:H films. The surface roughness, height and cluster grain sizes decrease with the temperature obtaining smoother films. All of this is a consequence of the hydrogen interaction with the growing surface. The total hydrogen in the film is reduced and hydrogen becomes more tightly bonded as temperature increases, which changes the way in which the nanocrystals are incorporated into the film and their environment. The nanocrystals average size is independent of the substrate temperature. The hydrogen passivating the nanocrystals for temperatures equal or higher than 240 °C present a bond breaking and diffusion process within the amorphous silicon matrix passivating the film more accurately and the hydrogen becomes more tightly bonded, leading to a more stable structure. The hydrogen atomic density is approximately 2×10^{22} atoms/cm^3 which is in the range of the a-Si:H. The optical properties of the films are directly related to the incorporation of hydrogen and whether it is weakly or tightly bonded, as is shown for the optical gap, absorption coefficient, n and k. A diminution of the optical gap of the pm-Si:H films is observed from 1.71 to 1.65 eV with the increase of the deposition temperature. A red-shift of the absorption coefficient, n and k with the deposition temperature is observed. Thus, a higher quality material with less hydrogen is obtained as the deposition temperature is increased. This is desirable for films related to solar cell devices development.

Acknowledgments

Authors thank M. A. Canseco, C. Flores for their experimental help and useful discussion. Thanks are also due to O. Jimenez and C. Gonzalez for information and technical support. We acknowledge partial financial support for this work from DGAPA-UNAM PAPIIT Projects IN108215, IN100914 and IN100213, CONACyT Mexico under project 179632, SENER-CONACyT project 151076. A

special acknowledgment is due to financial support from CONACyT through postdoctoral scholarship CVU 297213.

References

[1] U. Kroll, C. Bucher, S. Benagli, I. Schönbächler, J. Meier, A. Shah, J. Ballutaud, A. Howling, C. Hollenstein, A. Büchel, M. Poppeller, Thin Solid Films 451–452 (2004) 525–530.
[2] M.I. Kabir, S.A. Shahahmadi, V. Lim, S. Zaidi, K. Sopian, N. Amin, Int. J. Photoenergy 2012 (2012).
[3] D.L. Staebler, C.R. Wronski, Appl. Phys. Lett. 31 (1977) 292–294.
[4] K.H. Kim, E.V. Johnson, P. Roca i Cabarrocas, Sol. Energ. Mater. Sol. C 105 (2012) 208–212.
[5] D.E. Carlson, K. Rajan, Appl. Phys. Lett. 69 (1996) 1447–1449.
[6] B. Yan, G. Yue, L. Sivec, J. Yang, S. Guha, C.S. Jiang, Appl. Phys. Lett. 99 (2011) 113512.
[7] X. Multone, L. Fesquet, D. Borrello, D. Romang, G. Choong, E. Vallat-Sauvain, M. Charrière, A. Billet, J.-F. Boucher, J. Steinhauser, J.B. Orhan, R. Monnard, J. P. Cardoso, G. Charitat, B. Dehbozorgi, N. Guillot, G. Monteduro, M. Marmelo, R. Semenzi, S. Benagli, J. Meier, Sol. Energ. Mater. Sol. C 140 (2015) 388–395.
[8] P. Roca i Cabarrocas, A. Fontcuberta, S. Lebib, Y. Poissant, Pure Appl. Chem. 74 (2002) 359–367.
[9] M. Meaudre, R. Meaudre, R. Butte, S. Vignoli, C. Longeaud, J.P. Kleider, P. Roca i Cabarrocas, J. Appl. Phys. 86 (1999) 946.
[10] P. Roca i cabarrocas, N. Chaabane, A.V. Kharchenko, S. Tchakarov, Plasma Phys. Control. F 46 (2004) B235–B243.
[11] R. Butte, R. Meaudre, M. Meaudre, S. Vignoli, C. Longeaud, J.P. Kleider, P. Roca i Cabarrocas, Philos. Mag. B **79** (1999) 1079.
[12] A. Fontcuberta, H. Hofmeister, P. Roca i Cabarrocas, J. Non-Cryst. Solids 299-302 (2002) 284–289.
[13] N. Chaâbane, V. Suendo, H. Vach, P. Roca i Cabarrocas, Appl. Phys. Lett. 88 (2006) 203111.
[14] S. Lebib, P. Roca i Cabarrocas, Eur. Phys. J. Appl. Phys. 26 (2004) 17–27.
[15] K.H. Kim, E.V. Johnson, A. Abramov, P. Roca i Cabarrocas, Eur. Phys. J. PV 3 (2012) 30301.
[16] P. Roca i Cabarrocas, A. Fontcuberta, Y. Poissant, Thin Solid Films 403 (2002) 39–46.
[17] P. Roca i Cabarrocas, J.B. Chevrier, J. Huc, A. Lloret, J.Y. Parey, J.P.M. Schmith, J. Vac. Sci. Technol. **9** (1991) 2331.
[18] G.E. Jellison, F.A. Modine, Appl. Phys. Lett. 69 (1996) 371–374.
[19] A.R. Forouhi, I. Bloomer, Phys. Rev. B 34 (1986) 7018.
[20] A. Fontcuberta, P. Roca i Cabarrocas, C. Clerc, Phys. Rev. B 69 (2004) 125307.
[21] C. Goncalves, S. Charvet, A. Zeinert, M. Clin, K. Zellama, Thin solid Films 403-404 (2002) 91–96.
[22] S. Vepreck, F.A. Sarott, Z. Iqbal, Phys. Rev. B 36 (1987) 3344.
[23] F. Kail, S. Fellah, A. Abramov, A. Hadjadj, P. Roca i Cabarrocas, J. Non-Cryst. Solids 352 (2006) 1083–1086.
[24] M.Mayer, SIMNRA User's Guide, Version 6.04, (Max Planck-Institute für Plasmaphysik, Garching, 2008).
[25] H. Aguas, L. Raniero, L. Pereira, A.S. Viana, E. Fortunato, R. Martins, J. Non-Cryst. Solids 338–340 (2004) 183–187.
[26] D. Senouci, R. Baghdad, A. Belfedal, L. Chahed, X. Portier, S. Charvet, K.H. Kim, P. Roca i Cabarrocas, K. Zellama, Thin Solid Films 522 (2012) 186–192.
[27] F. Kail, J. Farjas, P. Roura, P. Roca i Cabarrocas, Phys. Rev. B 80 (2009) 073202.
[28] P. John, I.M. Odeh, M.J.K. Thomas, M.J. Tricker, J.I.B. Wilson, J.B.A. England, D. Newton, J. Phys. C: Solid State Phys. 14 (1981) 309–318.
[29] Y.F. Chen, Solid State Commun. 71 (1989) 1127–1130.
[30] R.W. Collins, J.M. Cavese, J. Non-Cryst. Solids 97–98 (1987) 269–272.
[31] M. Dürr, U. Höfer, Prog. Surf. Sci. 88 (2013) 61–101.
[32] E. Amanatides, D. Mataras, Surf. Coat. Tech. 205 (2011) 178–181.
[33] P. Roca i Cabarrocas, R. Cariou, M. Labrune, J. Non-Cryst. Solids 358 (2012) 2000–2003.
[34] P. Roca i Cabarrocas, J. Non-Cryst. Solids 266–269 (2000) 31–37.
[35] P. Roca i Cabarrocas, T. Nguyen-Tran, Y. Djeridane, A. Abramov, E.V. Johnson, G. Patriarche, J. Phys. D: Appl. Phys. 40 (2007) 2258.
[36] P. Roca i Cabarrocas, Y. Djeridane, T. Nguyen-Tran, E.V. Johnson, A. Abramov, Q. Zhang, Plasma Phys. Control. F 50 (2008) 124037.
[37] N. Bernhard, G.H. Bauer, W.H. Bloss, Prog. Photovolt: Res. Appl. 3 (1995) 149–176.
[38] W. Beyer, Sol. Energ. Mater. Sol. C 78 (2003) 235–267.
[39] T.Zimmermann, High-rate growth of hydrogenated amorphous and microcrystalline silicon for thin-film silicon solar cells using dynamic very-high frequency plasma-enhanced chemical vapor deposition, (Forschungszentrum Jülich, 2013).
[40] Y. Xu, X. Liao, G. Kong, X. Zeng, Z. Hu, H. Diao, S. Zhang, J. Cryst. Growth 256 (2003) 27–32.
[41] M.Netrvalová, M. Fischer, J. Mullerová, M. Zeman, and P.Šutta, Advanced Semiconductor Devices & Microsystems (ASDAM), 2010 8th International Conference proceedings, 329, 25–27 (2010).
[42] J.C. van den Heuvel, M.J. Geerts, J.W. Metselaar, Sol. Energy Mater. 22 (1991) 185–194.
[43] G.D. Cody, C.R. Wronski, B. Abeles, R.B. Stephens, B. Brooks, Solar Cells 2 (1980) 227–243.
[44] M. Vaněček, J. Fric, R.S. Crandall, A.H. Mahan, J. Non-Cryst. Solids 164–166 (1993) 335–338.